AGU PUBLICATIONS

Geophysical Research Letters

RESEARCH LETTER
10.1002/2016GL069133

Key Points:
- First report on double-peak subauroral ion drifts (DSAIDs)
- DSAIDs are regional and vary greatly with magnetic local time
- Double-layer R2-FACs may be the main driver of DSAIDs

Correspondence to:
X.-X. Zhang,
xxzhang@cma.gov.cn

Citation:
He, F., X.-X. Zhang, W. Wang, and B. Chen (2016), Double-peak subauroral ion drifts (DSAIDs), *Geophys. Res. Lett.*, *43*, 5554–5562, doi:10.1002/2016GL069133.

Received 13 APR 2016
Accepted 19 MAY 2016
Accepted article online 22 MAY 2016
Published online 4 JUN 2016

Double-peak subauroral ion drifts (DSAIDs)

Fei He[1], Xiao-Xin Zhang[2], Wenbin Wang[3], and Bo Chen[1]

[1]Changchun Institute of Optics, Fine Mechanics, and Physics, Chinese Academy of Sciences, Changchun, China, [2]Key Laboratory of Space Weather, National Center for Space Weather, China Meteorological Administration, Beijing, China, [3]High Altitude Observatory, National Center for Atmospheric Research, Boulder, Colorado, USA

Abstract This paper reports double-peak subauroral ion drifts (DSAIDs), which is unique subset of subauroral ion drifts (SAIDs). A statistical analysis has been carried out for the first time with a database of 454 DSAID events identified from Defense Meteorological Satellite Program observations from 1987 to 2012. Both case studies and statistical analyses show that the two velocity peaks of DSAIDs are associated with two ion temperature peaks and two region-2 field-aligned currents (R2-FACs) peaks in the midlatitude ionospheric trough located in the low-conductance subauroral region. DSAIDs are regional and vary significantly with magnetic local time. DSAIDs can evolve from/to SAIDs during their lifetimes, which are from several minutes to tens of minutes. Comparisons between the ionospheric parameters of DSAIDs and SAIDs indicate that double-layer region-2 field-aligned currents (R2-FACs) may be the main driver of DSAIDs. It is also found that DSAIDs happen during more disturbed conditions compared with SAIDs.

1. Introduction

During geomagnetic substorms, especially during their recovery phases, an intense ion convection zone with latitudinally narrow and longitudinally elongated rapid westward ion drifts (WID) or strong poleward electric fields (PEF) usually appears in the evening to midnight sector equatorward of the auroral oval. It was first termed as subauroral ion drifts (SAID) by *Spiro et al.* [1979]. More recently, *Foster and Burke* [2002] suggested an inclusive name, subauroral polarization streams (SAPS), to encompass both the narrow and intense SAIDs and the broader regions of sunward subauroral plasma drifts during storm times reported by *Yeh et al.* [1991]. SAPS may or may not contain the narrow, intensive, and dynamic SAIDs. SAIDs have been studied in both ground and space-based observations, such as in electric field measurements [*Maynard et al.*, 1980; *Karlsson et al.*, 1998; *Figueiredo et al.*, 2004; *Puhl-Quinn, et al.*, 2007], radar measurements [*Yeh et al.*, 1991; *Foster et al.*, 1994], and ion drift measurements [*Spiro et al.*, 1979; *Anderson et al.*, 1991, 1993, 2001]. To date, the generally accepted characteristics of SAIDs are as follows:

1. SAIDs are latitudinally confined and longitudinally extended WIDs located equatorward of the auroral oval. They sometimes overlap with the equatorial boundary of electron precipitation.
2. SAIDs have a single WID peak with a magnitude exceeding 1 km/s [*Anderson et al.*, 1991; *Rodger et al.*, 1992] or a single PEF peak exceeding 30 mV/m [*Karlsson et al.*, 1998; *Figueiredo et al.*, 2004]. There are also reports of the occurrence of eastward SAIDs [*Voiculescu and Roth*, 2008]. The latitudinal profile of drift velocity is similar to a single peak Gaussian function.
3. SAIDs happen mostly near ~60° magnetic latitude (MLAT) and ~2200 magnetic local time (MLT), and with a full width at half maximum (FWHM) between 0.05° and 2.0° [*Karlsson et al.*, 1998; *Figueiredo et al.*, 2004; *He et al.*, 2014].
4. High correlations between the MLATs of SAIDs and the downward region 2 field-aligned currents (R2-FACs) and between the FWHM of SAIDs and the density of R2-FACs [*He et al.* 2014] indicate that R2-FACs play an important role in the generation and evolution of SAIDs.
5. The occurrence, shape, and geomagnetic activity variations of SAIDs have a significant north-south asymmetry [*Zhang et al.*, 2015].

Although the one peak, spike structure has been observed in most of the SAID/SAPS events, different latitudinal structures of WIDs of SAIDs are also reported. *Mishin et al.* [2003] showed the electromagnetic wave structures within SAPS with a frequency range of ~0.15 Hz. They proposed several causal mechanisms for interpreting the wave structures, such as the cavity mode, ring current source, and magnetosphere-ionosphere (M-I) coupling. *Mishin and Blaunstein* [2008] and *Makarevich and Bristow* [2014] also reported wave structures in the SAPS (SAIDs). These results were case studies and focused mainly on the electromagnetic wave structures in the

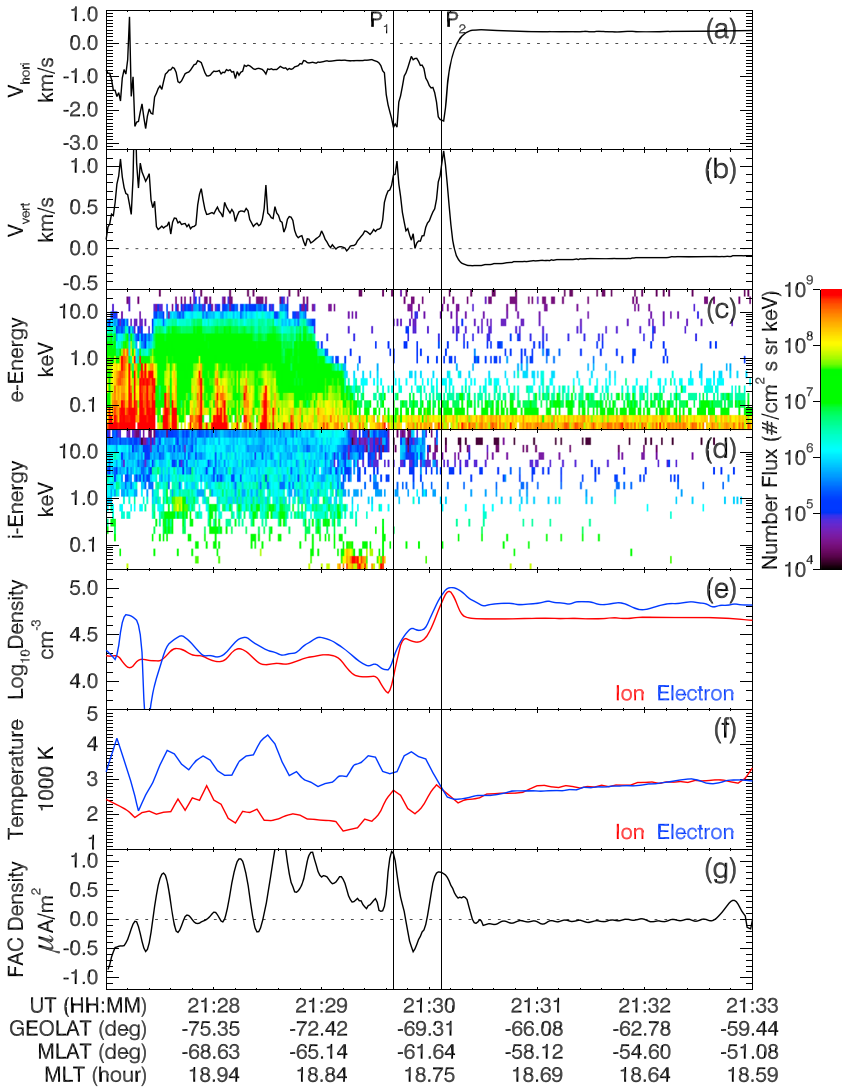

Figure 1. A DSAID event observed by the DMSP F13 satellite on 27 February 2004. (a) The horizontal drift velocities with negative values for westward, (b) the vertical drift velocities with positive values for upward, (c) the logarithmic scaled number fluxes of precipitation electrons and (d) ions with color bar shown at the right, (e) the logarithmic scaled ion/electron (red/blue) densities, (f) the ion/electron (red/blue) temperatures, and (g) FAC density with positive values downward and negative for upward, respectively. The two vertical lines indicate the two WID peaks of the DSAID event.

SAPS/SAIDs, which is just one type of the latitudinal variation of WIDs in SAPS/SAIDs. In this paper, we use DSMP satellite observations to show the latitudinally double-peaked SAIDs (DSAIDs), which have not been reported or studied before.

2. Observations and Discussion

2.1. Overview of DSAID Events

For over 25 years Defense Meteorological Satellite Program (DMSP) satellites have been monitoring the plasma parameters in the middle and high latitudes with a great success, using the ion drift meter (IDM) to measure the ion drift velocity, the retarding potential analyzer (RPA) to measure the ion density [*Greenspan et al.*, 1986], the precipitating energetic particle spectrometer (Special Sensor Precipitating Electron and Ion Spectrometer (SSJ)/4 and SSJ/5) to measure precipitating ion/electron fluxes[*Hardy et al.*, 1984], and the special sensor magnetometer (SSM) to measure the magnetic fields [*Rich et al.*, 1985]. Based on the long-term DMSP observations in the subauroral ionosphere, a large database of SAIDs from 1987 to

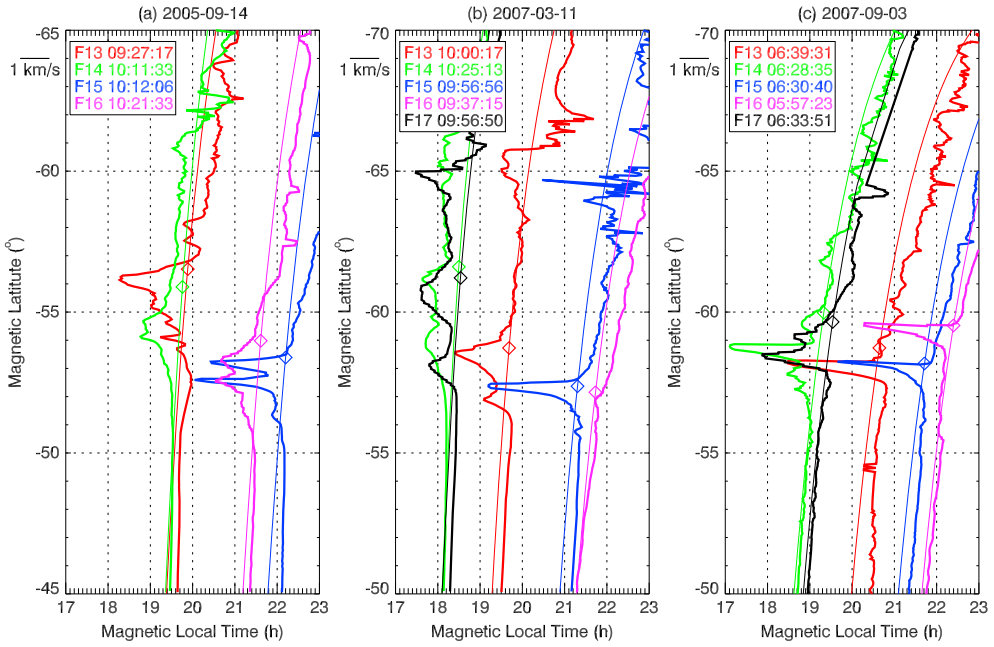

Figure 2. (a–c) Simultaneous observations of the horizontal drift velocities (thick lines, left to be westward) of DSAID events along DMSP satellite paths (thin lines). The colors for different satellites and the DSAID/SAID encountering times are shown at the upper left corners of each panel. Diamonds represent the equatorial boundaries of electron precipitation according to SSJ observations.

2012 has been built by *He et al.* [2014]. Apart from the typical single-peak SAID events, 454 DSAID events with two WID peaks in latitude are found in the DMSP observations from 1987 to 2012. An example of a DSAID event observed by the DMSP F13 satellite on 27 February 2004 is shown in Figure 1.

Two strong WID peaks were clearly seen in Figure 1 with one peak occurred at 21:29:40 UT and located at −62.8° MLAT, 1847 MLT with a velocity peak of −2.5 km/s and FWHM of 0.36° (P_1) and the other occurred at 21:30:06 UT and located at −61.3° MLAT, 1845 MLT with a velocity peak of −2.3 km/s and FWHM of 0.51° (P_2). Figure 1a also shows that each peak corresponded to an upward ion drift (UID) peak (Figure 1b), an ion temperature peak (Figure 1f), and a R2-FACs peak (Figure 1g), respectively. Both P_1 and P_2 were located equatorward of the equatorial boundary of the precipitation electrons and ions as shown in Figures 1c and 1d. They were also located in the midlatitude ionospheric trough (MIT) region as indicated in Figure 1e.

2.2. Regional and Temporal Variations of DSAIDs

Simultaneous observations by multiple DMSP satellites further show that DSAIDs have strong regional and temporal variations as demonstrated in Figure 2. The characteristics in Figure 2 for three DSAID events are as follows:

1. The magnitudes of the two WID peaks of DSAIDs may be approximately the same (Figure 2a, blue and purple) or significantly different. There were cases that the poleward peaks were greater (Figure 2b, red and black), and cases that the equatorward peaks were greater (Figure 2c, green and black).
2. DSAID events occurred and were significant in limited MLT sectors, e.g., after ~21.0 h in Figure 2a, or before ~20.0 h in Figures 2b and 2c. In other MLT sectors, however, the WID profiles still exhibited as SAIDs. This implies that the generation of DSAIDs may be due to the regional or localized irregular condition in the ionosphere and/or magnetosphere.
3. The profiles of DSAID varied greatly with MLT. In Figure 2a, the DSAID events observed by F15 and F16 were within 10 min, with a MLT difference of ~0.6 h. The MLATs and the latitudinal distances of the DSAID peaks were almost the same for both F15 and F16, but the DSAID peak velocities observed by F15 were almost 3 times larger than those seen by F16. For the simultaneous observations by F13, F15, and F17 at ~10:00 UT in Figure 2b, the double-peak structures were significant for F13 and F17 with similar magnitudes but different in MLATs and latitudinal distances. The magnitudes of the poleward

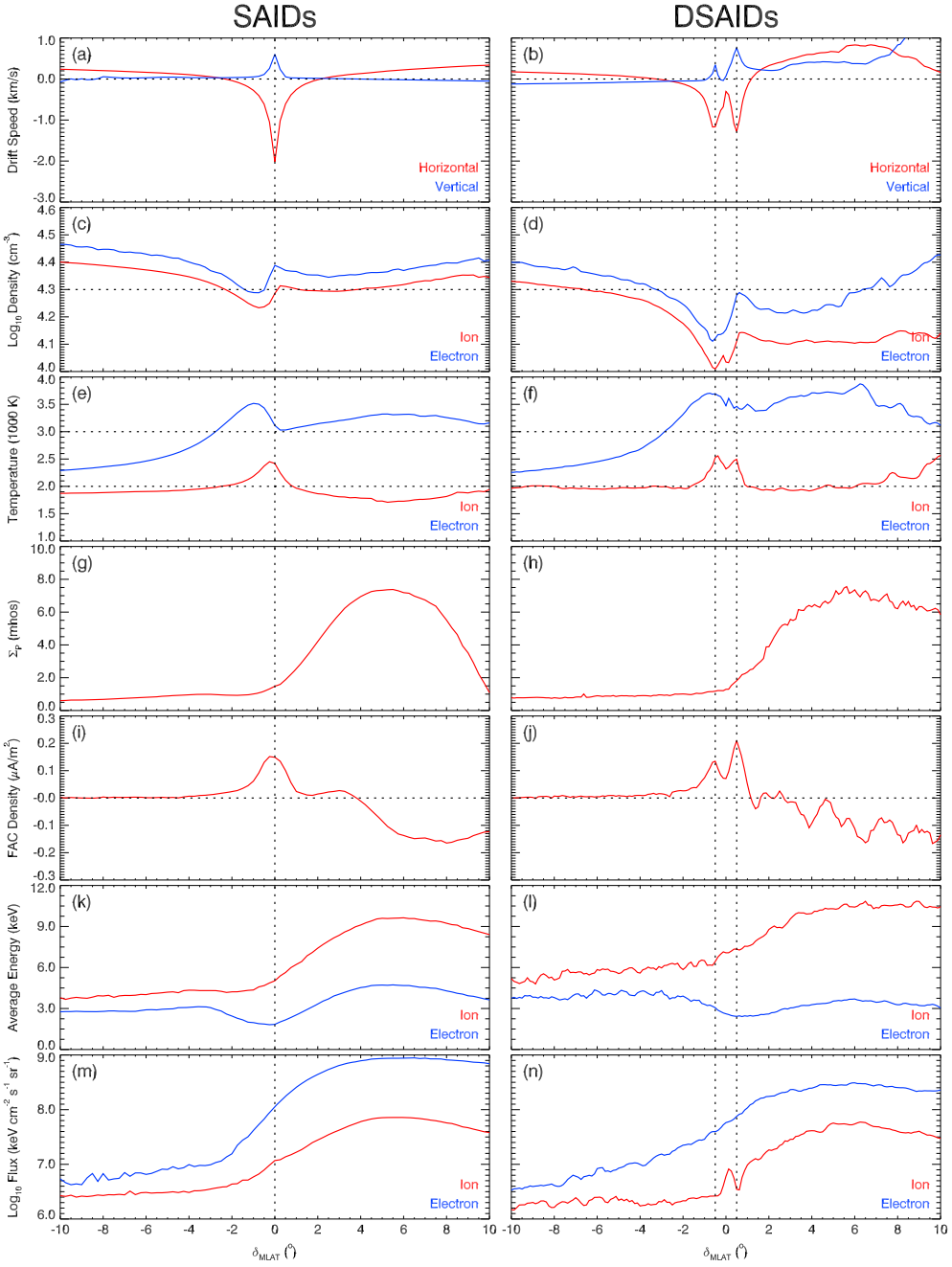

Figure 3. A statistical comparison between (left column) SAIDs and (right column) DSAIDs. From top to bottom shown are (a and b) horizontal/vertical (red/blue) ion drift velocities with positive for eastward/upward and negative for westward/downward, (c and d) logarithmic scaled ion/electron (red/blue) densities, (e and f) ion/electron (red/blue) temperatures, (g and h) ionospheric conductances calculated by the average energy and total energy flux of the precipitating electrons using the method of *Robinson et al.* [1987], (i and j) FAC densities with positive for downward Region-2 FACs, (k and l) average energy of precipitation ions/electrons (red/blue), and (m and n) total number fluxes of precipitation ions/electrons (red/blue), respectively. Negative δ_{MLAT} denotes equatorward, and positive one denotes poleward. The single velocity peak of SAIDs in the left column is marked by the vertical dashed line at $\delta_{MLAT} = 0°$, and the double peaks of DSAIDs in the right column are marked by the two vertical dashed lines at $\delta_{MLAT} = -0.5°$ and $\delta_{MLAT} = 0.5°$, respectively.

peak for F13, F15, and F17 increased with MLT, while the magnitudes of the equatorward peak decreased with MLT. In Figure 2c, during the simultaneous observations by F13, F14, F15, and F17 around 06:30 UT, the double-peak structures were evident for F14 and F17, while the F13 and F15 profiles still exhibited as SAIDs.

4. The DSAIDs also varied with time with time scales of several minutes (green and black lines in Figure 2c) to tens of minutes (green and red lines in Figure 2a and green and black lines in Figure 2b). Such time scales are similar to those of SAPS/SAIDs reported by *Oksavik et al.* [2006].

After investigating the evolution of all the DSAID events, we found that the generation and evolution of DSAIDs can approximately be divided into two situations. The first one is that a strong SAID event with a single peak first appears in the MLT sector from evening to midnight. This single peak then splits into two peaks in some MLT sectors, such as before 20.0 h, or after 21.0 h, to form a DSAID. In other MLT sectors SAIDs still have a single velocity peak. During the recovering phase of the event, the two peaks may fade together or merge into a single peak and finally disappear when the events are completely recovered. About 90% of the DSAID events follow this sequence. The second case for the remaining ~10% of events is that a weak DSAID event with two small peaks first appear in almost all the MLT sectors, and the two peaks are then strengthened with time to become strong double-peaked westward flows of more than 1 km/s in some MLT sectors, while merge into one strong peak in other MLT sectors to form SAIDs. Both SAIDs and DSAIDs disappear in the recovery phase of the event.

2.3. Statistical Comparisons Between DSAIDs and SAIDs

To clearly demonstrate the characteristics of DSAIDs and their differences from SAIDs, statistical profiles of both SAID- and DSAID-related ionospheric plasma parameters are shown in Figure 3. The calculation or extraction methods of the plasma parameters from DMSP observations are described in detail in *He et al.* [2014]. The latitudinal profiles of SAIDs in the left column of Figure 3 are obtained using the method of *Zhang et al.* [2015]. The latitudinal profiles for DSAIDs are obtained by the following procedure. First, the average latitudinal distance (d_{ave}) between the two peaks of DSAIDs (e.g., latitudinal distance between the two vertical lines in Figure 1) for all the events is calculated, which equals to 1.1° (actually $d_{ave} = 1.0°$ is adopted here to simplify the following analysis process). The center of the two peaks is taken as the central MLAT ($\delta_{MLAT} = 0°$) to normalize the latitudinal distances of the two peaks of DSAIDs to make the equatorward peak located at $\delta_{MLAT} = -0.5°$ and the poleward located at $\delta_{MLAT} = 0.5°$. Then all the normalized latitudinal profiles of the ionospheric plasma parameters are resampled into the MLAT grids of 0.125° interval between $\delta_{MLAT} = -10°$ and $\delta_{MLAT} = 10°$. Finally, the parameters in each grid are averaged to obtain the profiles in the right column of Figure 3. The characteristics in Figure 3 are summarized as the following:

1. SAIDs have a single WID peak (Figure 3a), corresponding to a single UID peak (Figure 2a), a single ion temperature peak (Figure 3e), and a single FAC density peak (Figure 3i). All of them are located at the poleward boundary of the MIT (Figure 3c) and the equatorward boundary of precipitation ions/electrons (Figures 3g, 3k, and 3m), in agreement with previous studies [*He et al.*, 2014, and references therein].
2. DSAIDs have two WID peaks (Figure 3b), corresponding to two UID peaks (Figure 3b), two ion temperature peaks (Figure 3f), and two FAC density peaks (Figure 3j). All of them are located at the equatorward boundary of precipitation ions/electrons (Figures 3h, 3l, and 3n). The peak at $\delta_{MLAT} = -0.5°$ is located at the center of the MIT, whereas the peak at $\delta_{MLAT} = 0.5°$ is located at the poleward boundary of the MIT (Figure 3c).
3. Both ion/electron densities of SAIDs are higher than those of DSAIDs (Figures 3c and 3d). The MIT is deeper for DSAIDs. The electron temperature for DSAIDs is ~500 K higher than that of SAIDs (Figures 3e and 3f), but the ion temperatures of SAIDs and DSAIDs are roughly the same.
4. Both SAIDs and DSAIDs are located in the low-conductance region of the MIT, which is equatorward of the electron auroral precipitation boundary (Figures 3g and 3h and 3k–3n). The latitudinal variations of the conductance and the average energy and total number flux of precipitation ions/electrons are similar, but the magnitude of the number flux of precipitating electrons for SAIDs is greater than that of DSAIDs. There is a small flux peak at $\delta_{MLAT} = \sim 0°$ for precipitating ions for DSAIDs (Figure 3n).
5. For both SAIDs and DSAIDs, the electron temperature has a single peak within the MIT, in agreement with *Moffett et al.* [1998] and *Förster et al.* [1999]. The ion temperature peaks are aligned with the WID peaks. Thus, there are two ion temperature peaks for DSAIDs, and both peaks are located poleward of the electron temperature peak. The electron temperatures are generally greater than the ion temperatures for both SAIDs and DSAIDs. The electron-ion temperature differences are ~1000 K in the WID regions.

Figure 4 further shows the differences between the occurrences of DSAIDs and SAIDs. It is noted in Figures 4a and 4b that both peaks of DSAIDs happen more equatorward and earlier in MLT than the single peak of

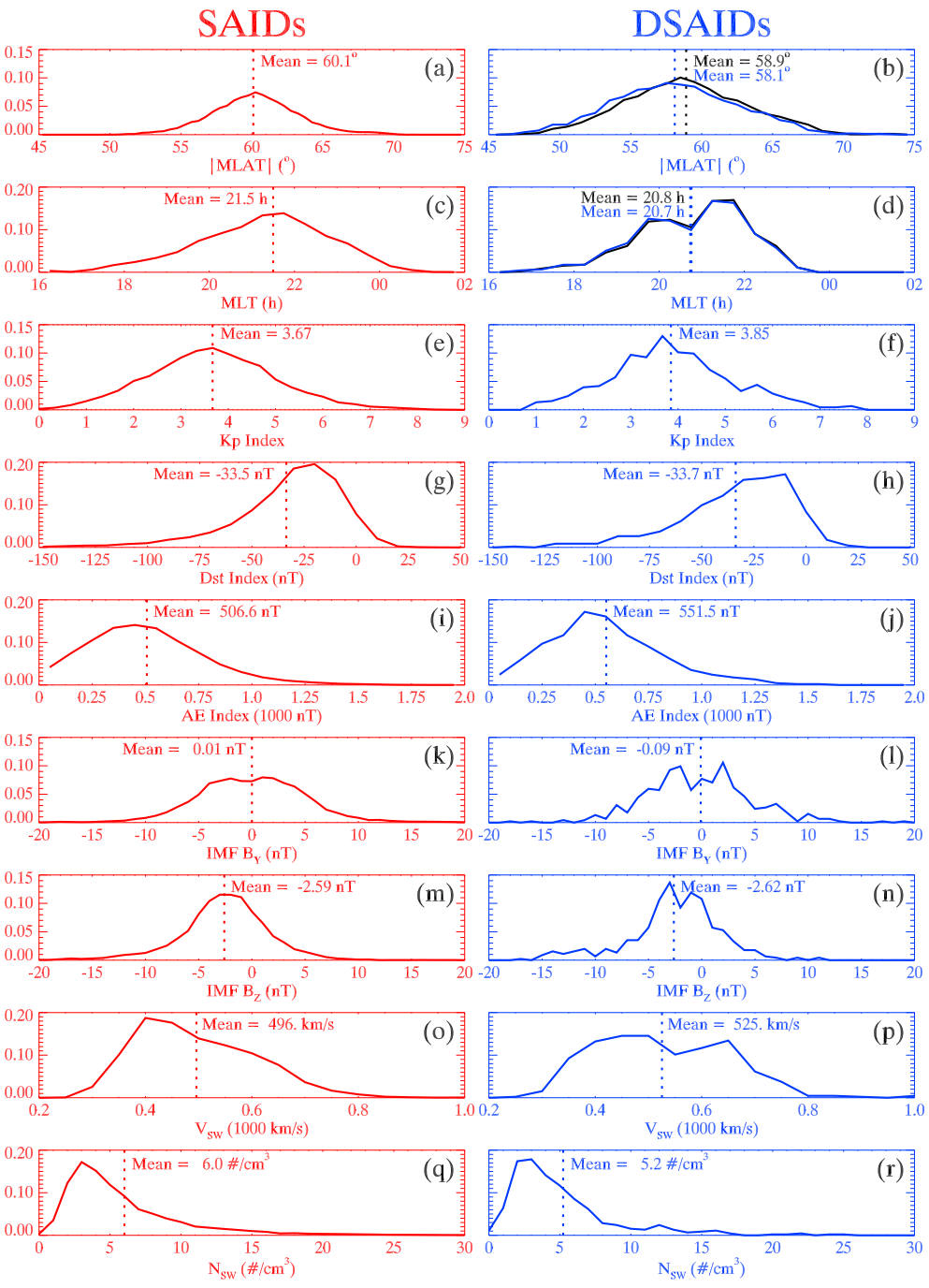

Figure 4. Occurrence probabilities of (left column) SAIDs and (right column) DSAIDs versus different variables. From top to bottom shown are (a and b) |MLAT|, the absolute value of MLAT binned in 0.5° intervals; (c and d) MLT binned in 0.5 h intervals; (e and f) the *Kp* index binned in 1/3 intervals; (g and h) the *Dst* index binned in 10 nT intervals; (i and j) the *AE* index binned in 100 nT intervals, (k and l) IMF B_y binned in 1 nT intervals; (m and n) IMF B_z binned in 1 nT intervals; (o and p) solar wind speed (V_{SW}) binned in 50 km/s intervals; and (q and r) solar wind number density (N_{SW}) binned in 1 cm^{-3} intervals. The vertical dashed lines represent the statistical means. The probabilities are obtained by dividing the event numbers in each bin with the number of total events. The black/blue lines in Figures 4b and 4d represent the poleward/equatorward peaks of the DSAIDs, respectively.

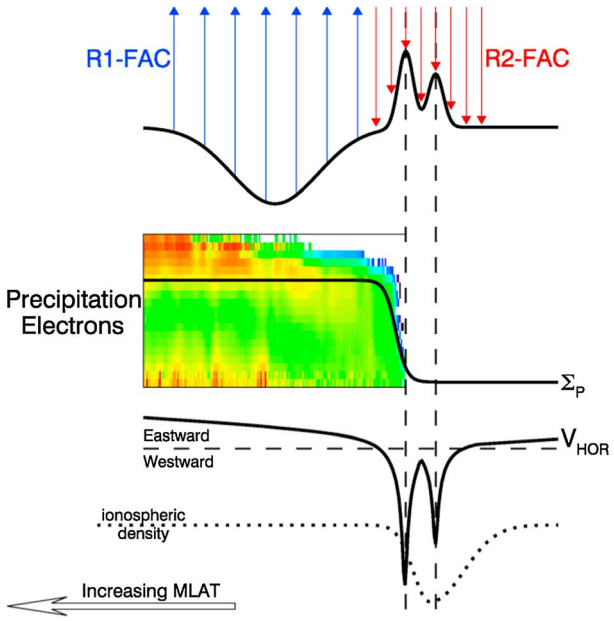

Figure 5. A schematic plot of the production mechanism of DSAIDs associated with FACs (solid arrows), precipitation electrons, height-integrated Pedersen conductance (Σ_P), horizontal ion drift velocity (V_{HOR}), and ionospheric electron densities (dotted line). The two WID peaks of the DSAID are marked by the two vertical dashed lines. R1-FAC denotes upward region-1 FACs, and R2-FAC denotes downward region-2 FACs.

SAIDs. This is mostly related to the fact that DSAIDs usually occur under geomagnetically more active conditions, as the average values of the *Kp* index (Figure 4c), *AE* index (Figure 4e), and solar wind speed (Figure 4h) for DSAIDs are slightly higher than those for SAIDs. However, the interplanetary magnetic field (IMF) conditions (Figures 4f and 4g) for DSAIDs and SAIDs do not have large differences, and IMF B_z is mainly southward for both DSAIDs and SAIDs (more than 80% of the events).

2.4. Preliminary Discussion on the DSAID Production Mechanism

The mechanisms for the occurrence of DSAIDs are evidently complicated and need further observational and theoretical studies. Here in Figure 5 we schematically outline a possible physical process for the production of DSAIDs.

The correlation between the PEFs or the WIDs and the R2-FACs has been well established using many satellite observations from different altitudes in the subauroral ionosphere [*Smiddy et al.*, 1977; *Maynard*, 1978; *Rich et al.*, 1980; *Ishii et al.*, 1992; *Lühr et al.*, 1994; *Anderson et al.*, 2001; *Figueiredo et al.*, 2004; *He et al.*, 2014]. Under geomagnetically disturbed conditions, the strongest partial ring currents are in the dusk to midnight sector [*Liemohn et al.*, 2001; *Le et al.*, 2004] and a large azimuthal gradient of the ring current pressure can lead to relatively strong R2-FACs [*Zheng et al.*, 2008]. Furthermore, the energetic ring currents overlap with the cold plasmasphere where wave instabilities develop [*Jordanova et al.*, 1996]. Under such circumstance, double-layer structures of R2-FACs may be generated in the localized region in the dusk to midnight sector possibly due to wave-particle interactions [*Sugiura*, 1984; *Lühr et al.*, 1994; *Jordanova et al.*, 1996]. When the energetic particles associated with the double-layer FACs precipitate into the ionosphere, frictional heating with neutral species (*e.g.*, N_2) in the subauroral region (O^+) can cause the double-peak signature of the ion temperature. Ion density is depleted due to the main loss mechanisms of ion-neutral chemical reaction ($N_2 + O^+ \rightarrow N + NO^+$) and dissociative recombination ($NO^+ + e^- \rightarrow N + O$) [*Anderson et al.*, 1993]. Finally, the density, temperature, and conductance gradients in the MIT region [*Keskinen et al.*, 2004] induce the double-peak structure of DSAID.

The statistical characteristics of SAIDs and DSAIDs indicate that the sources of SAIDs/DSAIDs may be the magnetospheric current generator. The large azimuthal gradients in the ion pressure in the equatorial plane drive relatively large FACs. Wave-particle interactions may generate multilayer structures of FACs. The ionospheric electric fields adjust accordingly to provide the current flow required by the magnetosphere when the FACs flow into the ionosphere in the low-conductance region associated with the MIT. If given downward FACs are not sufficient to return all the ionospheric Pedersen current in the region of low conductance, the current might be forced to develop another channel, leading to multiple circuits each of which generates large subauroral poleward electric fields and subsequent strong westward ion drifts. That is, the ionosphere responds to the magnetospheric current generator and determines where and how the currents will close.

The subauroral ionosphere where many important boundaries or structures, such as the auroral particle precipitation boundary, the plasmapause, the FACs, and the MIT, interact with each other is a very important region to understand the M-I coupling. The interactions between the ring currents and the plasmasphere

in the magnetosphere can greatly affect the dynamics of the subauroral ionosphere, generating significant WIDs and density trough, and these irregularities in turn can modify the dynamics of the plasmasphere and the thermosphere. The relationships between these boundary structures in the subauroral region need to be investigated in detail in the future to help us further our understanding of the M-I coupling.

3. Summary and Conclusion

In this letter, we show for the first time that some of subauroral ion drifts are associated with evident double-peak structures. The most outstanding signature of DSAIDs is their two significant WID peaks that are associated with two R2-FACs peaks. These two peaks are also associated with two ion temperature peaks in the MIT region, which is equatorward of the auroral oval. Simultaneous observations by multiple DMSP satellites reveal that DSAIDs are regional structures with time scales of a few minutes to tens of minutes. Statistical studies also show that DSAIDs usually occur under more disturbed solar wind and geomagnetic conditions when compared with SAIDs. A preliminary discussion on the generation mechanism of DSAIDs suggests that the various structures (e.g., auroral boundary, MIT, FACs, and temperature peak) existing in the subauroral region are highly coupled and that the R2-FACs are the essential driver of the WID or PEF. Further investigations, however, are required to systematically study the relationships between the various boundary structures in the subauroral ionosphere and the occurrence of DSAIDs.

Acknowledgments
The authors sincerely thank NOAA/NESDIS/National Geophysical Data Center for the provision of the DMSP IDM, RPA, SSJ/4, and SSM data available from http://satdat.ngdc.noaa.gov/dmsp/data/. The *Kp*, *Dst*, and *AE* indices are available from the Kyoto World Data Center for Geomagnetism at http://wdc.kugi.kyoto-u.ac.jp/. The solar wind data are available from http://omniweb.gsfc.nasa.gov/ow_min.html. This work was supported by the National Natural Science Foundation of China (41204102 and 41274147), the National Basic Research Program of China (2012CB957800 and 2011CB811400), and the National Hi-Tech Research and Development Program of China (2012AA121000). The National Center for Atmospheric Research is sponsored by the National Science Foundation.

References

Anderson, P. C., R. A. Heelis, and W. B. Hanson (1991), The ionosphere signatures of rapid subauroral ion drifts, *J. Geophys. Res.*, *96*(A4), 5785–5792, doi:10.1029/90JA02651.

Anderson, P. C., W. B. Hanson, R. A. Heelis, J. D. Craven, D. N. Baker, and L. A. Frank (1993), A proposed production model of rapid subauroral ion drifts and their relationship to substorm evolution, *J. Geophys. Res.*, *98*(A4), 6069–6078, doi:10.1029/92JA01975.

Anderson, P. C., D. L. Carpenter, K. Tsuruda, T. Mukai, and F. J. Rich (2001), Multisatellite observations of rapid subauroral ion drifts (SAID), *J. Geophys. Res.*, *106*(A12), 29,585–29,599, doi:10.1029/2001JA000128.

Figueiredo, S., T. Karlsson, and G. T. Marklund (2004), Investigation of subauroral ion drifts and related field-aligned currents and ionospheric Pedersen conductivity distribution, *Ann. Geophys.*, *22*, 923–934, doi:10.5194/angeo-22-923-2004.

Foster, J. C., and W. J. Burke (2002), SAPS: A new categorization for sub-auroral electric fields, *Eos. Trans. AGU*, *83*(36), 393, doi:10.1029/2002EO000289.

Foster, J. C., M. J. Buonsanto, M. Mendillo, D. Nottingham, F. J. Rich, and W. Denig (1994), Coordinated stable auroral red arc observations: Relationship to plasma convection, *J. Geophys. Res.*, *99*(A6), 11,429–11,439, doi:10.1029/93JA03140.

Förster, M., J. C. Foster, J. Smilauer, K. Kudela, and A. V. Mikhailov (1999), Simultaneous measurements from the Millstone Hill radar and the Active satellite during the SAID/SAR arc event of the March 1990 CEDAR storm, *Ann. Geophys.*, *17*(3), 389–404, doi:10.1007/s00585-999-0389-6.

Greenspan, M. E., P. B. Anderson, and J. M. Pelagatti (1986), Characteristics of the thermal plasma monitor (SSIES) for the Defense Meteorological Satellite Program (DMSP) spacecraft S8 though S10 *Tech. Rep. AFGL-TR-86-0227*, Air Force Geophys. Lab., Hanscom Air Force Base, Mass.

Hardy, D. A., H. C. Yeh, L. K. Schmitt, T. L. Schumaker, M. S. Gussenhoven, A. Huber, F. J. Marshall, and J. Pantazis (1984), Precipitating electron and ion detectors (SSJ/4) on the block 5D/Flights 6–10 DMSP satellites: Calibration and data presentation *Tech. Rep. AFGL-TR-84-0317*, Air Force Geophys. Lab., Hanscom Air Force Base, Mass.

He, F., X.-X. Zhang, and B. Chen (2014), Solar cycle, seasonal, and diurnal variations of subauroral ion drifts: Statistical results, *J. Geophys. Res. Space Physics*, *119*, 5076–5086, doi:10.1002/2014JA019807.

Ishii, M., M. Sugiura, T. Iyemori, and J. A. Slavin (1992), Correlation between magnetic and electric field perturbations in the field-aligned current regions deduced from DE 2 observations, *J. Geophys. Res.*, *97*(A9), 13,877–13,887, doi:10.1029/92JA00110.

Jordanova, V. K., J. U. Kozyra, and A. F. Nagy (1996), Effects of heavy ions on the quasi-linear diffusion coefficients from resonant interactions with electromagnetic ion cyclotron waves, *J. Geophys. Res.*, *101*(A9), 19,771–19,778, doi:10.1029/96JA01641.

Karlsson, T., G. T. Marklund, L. G. Blomberg, and A. Mälkki (1998), Subauroral electric fields observed by the Freja satellite: A statistical study, *J. Geophys. Res.*, *103*(A3), 4327–4314, doi:10.1029/97JA00333.

Keskinen, M. J., S. Basu, and S. Basu (2004), Midlatitude sub-auroral ionospheric small scale structure during a magnetic storm, *Geophys. Res. Lett.*, *31*, L09811, doi:10.1029/2003GL019368.

Le, G., C. T. Russell, and K. Takahashi (2004), Morphology of the ring current derived from magnetic field observations, *Ann. Geophys.*, *22*, 1267–1295, doi:10.5194/angeo-22-1267-2004.

Liemohn, M. W., J. U. Kozyra, M. F. Thomsen, J. L. Roeder, G. Lu, J. E. Borovsky, and T. E. Cayton (2001), Dominant role of the asymmetric ring current in producing the stormtime *Dst**, *J. Geophys. Res.*, *106*, 10,883–10,904, doi:10.1029/2000JA000326.

Lühr, H., J. Warnecke, L. J. Zanetti, P. A. Lindqvist, and T. J. Hughes (1994), Fine structure of field-aligned current sheets deduced from spacecraft and ground-based observations: Initial FREJA results, *Geophys. Res. Lett.*, *21*(17), 1883–1886, doi:10.1029/94GL01278.

Makarevich, R. A., and W. A. Bristow (2014), Fine structure of subauroral electric field and electron content, *J. Geophys. Res. Space Physics*, *119*, doi:10.1002/2014JA019821.

Maynard, N. C. (1978), On large poleward-directed electric fields at sub-auroral latitudes, *Geophys. Res. Lett.*, *5*(7), 617–618, doi:10.1029/GL005i007p00617.

Maynard, N. C., T. L. Aggson, and J. P. Heppner (1980), Magnetospheric observation of large subauroral electric fields, *Geophys. Res. Lett.*, *7*(11), 881–884, doi:10.1029/GL007i011p00881.

Mishin, E. V., W. J. Burke, C. Y. Huang, and F. J. Rich (2003), Electromagnetic wave structures within subauroral polarization streams, *J. Geophys. Res.*, *108*(A8), 1309, doi:10.1029/2002JA009793.

Mishin, E. V., and N. Blaunstein (2008), Irregularities within subauroral polarization stream-related troughs and GPS radio interference at midlatitudes, in *Midlatitude Ionospheric Dynamics and Disturbances*, *Geophys. Monogr. Ser.*, vol. 181, edited by P. M. Kintner Jr. et al., pp. 291–295, AGU, Washington, D. C.

Moffett, R., A. E. Ennis, G. J. Bailey, R. A. Heelis, and L. H. Brace (1998), Electron temperature during rapid subauroral ion drift events, *Ann. Geophys.*, *16*(4), 450–459, doi:10.1007/s00585-998-0450-x.

Oksavik, K., R. A. Greenwald, J. M. Ruohoniemi, M. R. Hairston, L. J. Paxton, J. B. H. Baker, J. W. Gjerloev, and R. J. Barnes (2006), First observations of the temporal/spatial variation of the sub-auroral polarization stream from the SuperDARN Wallops HF radar, *Geophys. Res. Lett.*, *33*, L12104, doi:10.1029/2006GL026256.

Puhl-Quinn, P. A., H. Matsui, E. Mishin, C. Mouikis, L. Kistler, Y. Khotyaintsev, P. M. E. Décréau, and E. Lucek (2007), Cluster and DMSP observations of SAID electric fields, *J. Geophys. Res.*, *112*, A05219, doi:10.1029/2006JA012065.

Rich, F. J., W. J. Burke, C. Kelley, and M. Smiddy (1980), Observations of field-aligned currents in association with strong convection electric fields at subauroral latitudes, *J. Geophys. Res.*, *85*(A5), 2355–2340, doi:10.1029/JA085iA05p02335.

Rich, F. J., D. A. Hardy, and M. S. Gussenhoven (1985), Enhanced ionosphere magnetosphere data from the DMSP satellites, *Eos. Trans. AGU*, *66*(26), 513–514, doi:10.1029/EO066i026p00513.

Robinson, R. M., R. R. Vondark, K. Miller, T. Dabbs, and D. Hardy (1987), On calculating ionospheric conductances from the flux and energy of precipitating electrons, *J. Geophys. Res.*, *92*(A3), 2565–2569, doi:10.1029/JA092iA03p02565.

Rodger, A. S., R. J. Moffett, and S. Quegan (1992), The role of ion drift in the formation of ionization troughs in the mid- and high-latitude ionosphere: A review, *J. Atmos. Sol. Terr. Phys.*, *54*(1), 1–30, doi:10.1016/0021-9169(92)90082-V.

Smiddy, M., M. C. Kelley, W. Burke, F. Rick, R. Sagalyn, B. Shuman, R. Hays, and S. Lai (1977), Intense poleward-directed electric fields near the ionospheric projection of the plasmapause, *Geophys. Res.Lett.*, *4*(11), 543–546, doi:10.1029/GL004i011p00543.

Spiro, R. W., R. H. Heelis, and W. B. Hanson (1979), Rapid subauroral ion drifts observed by Atmospheric Explorer C, *Geophys. Res. Lett.*, *6*(8), 657–660, doi:10.1029/GL006i008p00657.

Sugiura, M. (1984), A fundamental magnetosphere-ionosphere coupling mode involving field-aligned currents as deduced from DE-2 observations, *Geophys. Res.Lett.*, *1*(9), 877–880, doi:10.1029/GL011i009p00877.

Voiculescu, M., and M. Roth (2008), Eastward sub-auroral ion drifts or ASAID, *Ann. Geophys.*, *26*, 1955–1963, doi:10.5194/angeo-26-1955-2008.

Yeh, H.-C., J. C. Foster, F. J. Rich, and W. Swider (1991), Storm time electric field penetration observed at mid-latitude, *J. Geophys. Res.*, *96*(A4), 5707–5721, doi:10.1029/90JA02751.

Zhang, X.-X., F. He, W. Wang, and B. Chen (2015), Hemispheric asymmetry of subauroral ion drifts: Statistical results, *J. Geophys. Res. Space Physics*, *120*, 4544–4554, doi:10.1002/2015JA021016.

Zheng, Y., P. C. Brandt, A. T. Y. Lui, and M. C. Fok (2008), On ionospheric trough conductance and subauroral polarization streams: Simulation results, *J. Geophys. Res.*, *113*, A04209, doi:10.1029/2007JA012532.